# Parametric study of the acceleration layer in a high power Hall effect thruster by Fabry-Pérot spectroscopy

**IEPC-2005-144**

*Presented at the 29th International Electric Propulsion Conference, Princeton University, October 31 – November 4, 2005*

D. Gawron* and S. Mazouffre†
*Laboratoire d'Aérothermique, CNRS, 1c avenue de la recherche scientifique, 45071 Orléans, France*

C. Boniface‡
*CPAT, CNRS, Université Paul Sabatier, 118 route de Narbonne, 31062 Toulouse, France*

**Abstract: The flow velocity of singly charged xenon ion is determined by means of Fabry-Pérot interferometry at the exhaust of a laboratory-model PPS X000 Hall effect thruster by analyzing the Doppler shifted spectral profile of the 541.91 nm $Xe^+$ ion line. A technique combining numerical simulations and CCD imaging is used to readjust the obtained velocity profiles in space, as this information is lost because of the signal integration in space during measurements. The applied voltage was varied from 200 V to 1000 V, whereas the xenon mass flow rate was varied from 5 mg.s$^{-1}$ to 15 mg.s$^{-1}$ to investigate the evolution of both the ion speed and the distribution of the accelerating potential. Finally, the presence of low velocity ions in the plasma plume has been highlighted.**

## Nomenclature

$dV$ = elementary volume
$e$ = elementary charge
$I$ = Fabry-Pérot signal intensity
$I_d$ = discharge current
$\vec{k}$ = wave vector
$m_{Xe}$ = Xe atomic mass
$n$ = $Xe^+$ ions density
$P$ = $Xe^+$ spectral lineshape at 541.9 nm
$\vec{r}$ = vector locating an elementary volume element
$T$ = gas temperature
$U_{acc}$ = accelerating potential
$U_d$ = applied voltage
$v$ = $Xe^+$ ions velocity
$v_{axial}$ = axial component of the Xe+ ions velocity vector
$v_{radial}$ = radial component of the Xe+ ions velocity vector
$v_{projected}$ = projection of the Xe+ ions velocity vector over the line of sight
$\alpha$ = angle between the thruster axis and a given velocity vector
$\theta$ = angle between the setup line of sight and the thruster axis (= 59°)
$\lambda_0$ = wavelength of the studied line (= 541.9 nm)
$\lambda$ = wavelength
$\upsilon_0$ = frequency of the studied line (= 553.6 THz)
$\upsilon$ = frequency
$\Phi_a$ = xenon mass flow rate

* phD student, CNRS, gawron@cnrs-orleans.fr
† Research scientist, CNRS, mazouffre@cnrs-orleans.fr
‡ phD student, CNRS, boniface@cpat.ups-tlse.fr

## I. Introduction

Determination of singly ionized xenon ion velocity in a Hall effect thruster plasma plume furnishes with valuable information about the thruster working conditions and overall performances. Indeed, the ion flow velocity is directly linked to the specific impulse, it mainly determines the thrust, and it participates in the engine efficiency. Furthermore, the local plasma potential and electric field can be derived from a measurement of the ion velocity map. Laser Induced Fluorescence spectroscopy seems to be particularly adapted to this study as it offers a set of matchless features. However, it is a cumbersome diagnostic tool that is not straightforward to implement onto ground-test facility dedicated to Hall effect thruster studies. Settling a non-intrusive diagnostic tool, which is less complicated in its utilization, yet complementary in its contribution, is essential in order to perform investigations of $Xe^+$ ion flow characteristics, whatever the thruster geometry and operating conditions. Fabry-Pérot interferometry, which is based on the analysis of light emitted by the plasma, fulfills all requirements in order to be employed as a routine diagnostic tool, although it is inferior to LIF spectroscopy from a standpoint of spectral as well as spatial resolution. Nevertheless, Fabry-Pérot interferometry allows to measure the ion velocity with good accuracy when changing thruster parameters, in such a way that a large data set can be easily collected. Moreover, such a tool can be used while performing others measurements like electromagnetic waveform acquisition with antennas and CCD camera imaging, only to name a few. In this contribution, we present measurements of the $Xe^+$ ion axial velocity realized within the plasma of a high power laboratory-model PPS X000 Hall effect thruster by means of Fabry-Pérot spectroscopy. All reported measurements have been carried out by studying the spectral profile of the 541.91 nm $Xe^+$ line.

## II. Experimental setup

A Fabry-Pérot (FP) interferometer must be regarded as a very narrow bandwidth optical filter. It is often used to examine the detailed structure of spectral lines. [1, 2] A schematic view of the complete Fabry-Pérot system used for works discussed in this paper is depicted in Fig.1. After being collected with a lens, light emanating from the thruster xenon plasma is transported towards the optical bench by means of a multimode silica step index optical fiber with a 365 µm core diameter. The light leaving the fiber is collected with a 400 mm focal distance lens in such a way that a collimated beam of light is created. The parallel beam passes a plane Fabry-Pérot cavity limited by two 2.5 cm diameter apertures. The cavity mirror coating is optimized for wavelengths ranging from 450 nm to 550 nm. Behind the cavity, the transmitted light is focused onto a 0.7 mm pinhole in order to solely select the central interference ring. The pinhole is imaged onto the entrance slit of a 40 cm monochomator that acts as a rough wavelength selector to separate the line to be studied from the remainder of the spectrum ($\Delta\lambda \sim 0.8$ nm). A photomultiplier tube (Hamamatsu R928) is used as a light detector. The delivered signal is registered with an oscilloscope. The Fabry-Pérot (RC110 from Burleigh) is a piezo-scanned type; the length as well as the alignment of the cavity is controlled by applying a high voltage onto piezoelectric mirror mounts. An accurate frequency scan is realized by smoothly varying the mirror position with a high voltage ramp. All measurements presented in this paper have been obtained with a cavity scanning frequency of 10 Hz. Each spectrum results from the average over 256 cycles.

The distance between the two dielectric mirrors of the Fabry-Pérot cavity is 3.0 mm, meaning that the Free Spectral Range of the cavity is equal to 50.0 GHz.[3] In the spectral domain of interest ($\lambda \sim 540$ nm), the mirror reflectivity is around 95.3%. The mirrors are flattened to $\lambda/200$. Therefore, the net finesse of the Fabry-Pérot cavity is around 62. The instrumental finesse that characterizes the resolving power of the complete FP bench by accounting for pinholes and lenses induced losses, is found to be around 59.[3] In other words, the setup allows to achieve a spectral resolution of about 0.75 GHz, i.e. 0.7 pm at 542 nm, as the light beam is perfectly collimated. The apparatus profile does not allow to resolve the complex structure of the Xe+ line, however, it is narrow enough to precisely measure Doppler shift. The strong Ne I line at 540.06 nm, which is emitted by a low-pressure neon lamp, is used to accurately align the Fabry-Pérot bench.

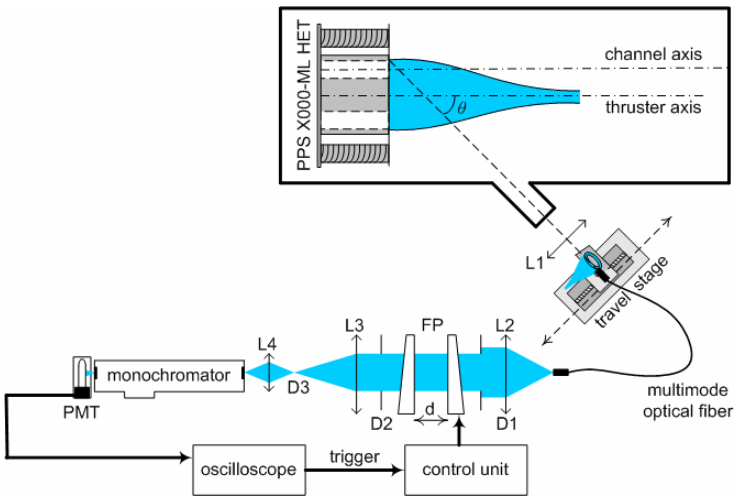


**Figure 1. Fabry-Pérot Experimental setup**

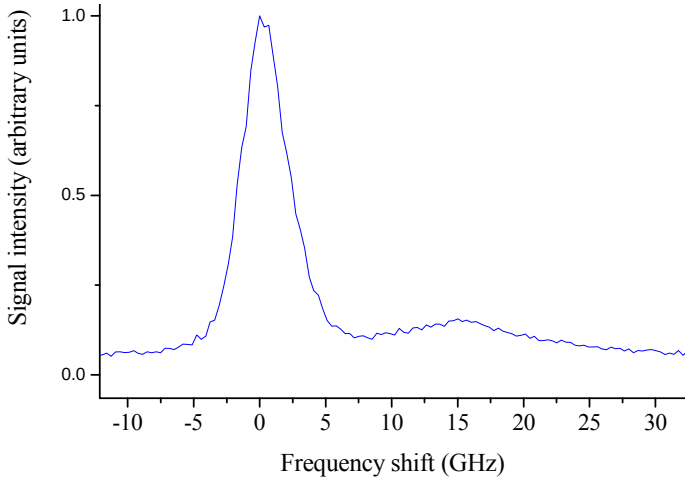


**Figure 2. Typical interference pattern measured by Fabry-Pérot interferometry**

The optical fiber collecting the light from the thruster has been mounted unto a Newport micrometric travel stage so that the optical fiber can be moved in the image plane of the collection lens (whose focal length is 100 mm). In other word, the setup allows to obtain different positions for the line of sight of the detection branch without moving the thruster. For the results discussed in this paper, the angle $\theta$ between the line of sight and the thruster axis is equal to 59°. The distance between the lens of the thruster being equal to 1.70 m, the optical magnification is 17. Since the fiber radius is equal to 365 µm, the detection branch collects photons from a ~7 mm diameter cylinder. The distance between the thruster and the lens is considered to be infinite so that it is not necessary to take the field depth into account for calculations (this has been checked experimentally).

A typical interference pattern obtained thanks to this setup is displayed in Fig.2. The presence of these two peaks being not straightforward, it has been necessary to use a theoretical model to extract data from the measurements.

## III. Data extraction

### A. Mathematical formalism

The shapes of the interference patterns are due to the integration of the plasma emissivity $\varepsilon$ along the line of sight:

$$I(\upsilon) = \int_{-\infty}^{+\infty}\int_{-\infty}^{+\infty}\int_{-\infty}^{+\infty} \varepsilon(\upsilon,\vec{r}) \cdot dV \tag{1}$$

with

$$\varepsilon(\nu,\vec{r}) \propto n(\vec{r}) \cdot P(\upsilon,\vec{r}) \tag{2}$$

The plasma temperature is of an order of magnitude of 800 K, which leads to a Doppler broadening equal to ~2.5 GHz (calculated by using Eq.5). In these conditions, the natural line width (~0.16 GHz) can be neglected, so that $P$ can be approximated by a Gaussian function:

$$P(\upsilon,\vec{r}) \propto \frac{1}{\Delta\upsilon_D(\vec{r})} \cdot e^{-4\cdot\ln(2)\cdot\left(\frac{\upsilon-\delta\upsilon_D(\vec{r})}{\Delta\upsilon_D(\vec{r})}\right)^2} \tag{3}$$

with

$$\delta\upsilon_D = \vec{k}\cdot\vec{v} \tag{4}$$

and

$$\Delta\upsilon_D = 7.162\times10^{-7}\times\upsilon_0\times\sqrt{\frac{T}{m_{Xe}}} \tag{5}$$

Therefore, an interference pattern contains information about the ions density, temperature through Doppler broadening $\Delta\upsilon_D$ and velocity through Doppler shift $\delta\upsilon_D$. As an approximation, the field depth is neglected since measurements have shown that from 1.50 m, the position of the light source did not have an influence on the signal intensity. Moreover, the medium is considered as fully transparent at 541.9 nm.

**B. Modeling the interference pattern shape**

As a first approximation, we considered that the plasma properties do not evolve axially, providing the studied volume is far enough from the thruster exit. Then, the only relevant dimension is the axial one. Since the $Xe^+$ ions density and velocity distribution are unknown, they have been simulated by Gaussian functions according to hybrid models developped in the CPAT of Toulouse. So by replacing the triple integral by a sum in Eq.1 we can obtain a crude model which is nevertheless able to reproduce roughly the general shape of the experimental interference patterns.[4] However, the conclusions of the cited paper were eroneous. Indeed, the first peak in the interference pattern (see Fig.2) is not due to the setup geometry but to the presence of low velocity ions in the plasma plume. Indeed, if the velocity and density distributions are Gaussian functions, then low velocity ions are mathematically introduced in the model if the width of the velocity function is narrower than the density function width. The grey areas in Fig.3 represent the low velocity ions in such a configuration.

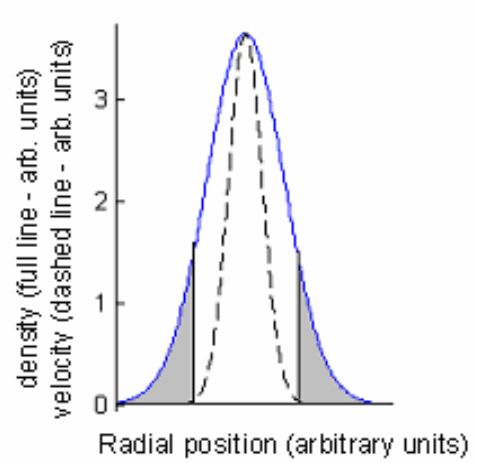


**Figure 3. Full line: radial density profile. Dashed line: radial velocity profile.**

It has been checked experimentally that this first peak is indeed not Doppler shifted. Therefore, an interference pattern contains two peaks; the first one (and usually the larger one) is linked to $Xe^+$ ions with low velocity whereas the second one corresponds to accelerated $Xe^+$ ions (see Fig.2).

Thus, providing that it is possible to determine the position of the elementary volume corresponding to the top of the Doppler shifted peak (i.e. the second one), the Doppler shift corresponding to the $Xe^+$ ion velocity can be measured simply by determining the distance between the two peaks (the FP interferometer free spectral range being equal to 50 GHz). However, according to Eq.4 this Doppler shift is produced by the projection of the ion velocity vector over the line of sight. Therefore, one has to make the assumption that the $Xe^+$ ion velocity is mainly axial near the channel axis (as defined in Fig.1).

This crude model shows the plasma plume has to contain $Xe^+$ ions with low velocity even though it is not known either if they are evenly distributed along the line of sight or display a strong density in a reduced volume. Note that in this model, the integration of the signal occurs along a line in the mathematical sense of the word. In reality, the signal integration occurs over a volume.

This one dimensional model also confirmed that the gas temperature influence on the interference pattern shape was negligible. However, in addition to its obvious inaccuracy, such a model is not valid anymore for elementary volumes close to the thruster exit, which is the area that is of the most interest. Therefore, a more complex model has been developed.

**C. Two dimensional modeling**

In order to reduce the number of unknown quantities, imaging by means of a CCD camera has been used in addition to Fabry-Pérot interferometry. The thruster was imaged at 90° from its axis, allowing to obtain a two dimensional $Xe^+$ ions density map after treatment of the picture by Abel transform. The scale of such a density map can only be relative, but this is relevant with Eq.2. With a two dimensional model, Gaussian functions are not good approximations enough to simulate the $Xe^+$ ion velocity distribution in space. The selected approach has been to consider the thruster plasma plume as an expansion jet with a given divergence angle $D$ originating from a single space point. This point is defined as the top of the divergence cone, and thus depends on $D$. Typically $D$ has been set to 30°, which places the point from which the jet originates at 43 mm inside the thruster channel. Therefore, even though such a point has no physical existence, it is expected that it is far enough inside the channel so that the selected approach gives satisfying results.

Each point can be localized by either its Cartesian coordinates $(z,r)$ or its polar coordinates $(\alpha,R)$. Angles are measured in a counterclockwise direction from the thruster axis and $R$ is the distance between the top of the divergence cone and the considered point.

In order to compute an interference pattern, the only points that are taken into account are those included both in the divergence cone and the area of sight. It means that several points are disregarded but their

contribution to the total density along the line of sight is typically less than 5%. Note that what is usually called line of sight is in fact a volume in reality, and an area in a two dimensional model. The width of this so-called line (or the diameter of the volume) can be estimated thanks to the detection branch magnification ($\gamma$ = 17) and the optical fiber diameter (365 µm), leading to a width of ~7 mm.

A velocity vector corresponds to each point included in the divergence cone. We have chosen to divide each velocity vector in its axial and radial components (i.e. horizontal and vertical components respectively for Fig.4). Then these components can be calculated for each point corresponding to the model calculation domain (i.e. the area at the intersection of the divergence cone and the line of sight) thanks to Eq.6 and Eq.7.

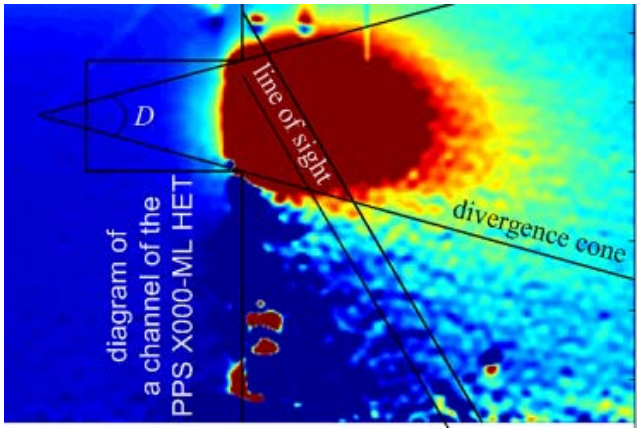


**Figure 4. Abel transform of a CCD picture of the PPS X000-ML plasma plume. The line of sight, the divergence cone and a diagram of the thruster are also sketched.**

$$v_{axial}(\alpha,R) = \frac{\left|\vec{v}(\alpha,R)\right| \cdot \cos(\alpha)}{\sqrt{1+\tan^2(\alpha)}} \tag{6}$$

$$v_{radial}(\alpha,R) = \sqrt{\left(\vec{v}(\alpha,R)\cdot\cos(\alpha)\right)^2 - v_{axial}^2(\alpha,R)} \qquad \text{if } \alpha < 0$$

$$v_{radial}(\alpha,R) = -\sqrt{\left(\vec{v}(\alpha,R)\cdot\cos(\alpha)\right)^2 - v_{axial}^2(\alpha,R)} \qquad \text{if } \alpha \geq 0 \tag{7}$$

The cosine in Eq.6 accounts for the ions energy decrease with the increasing distance from the channel axis.[5]

However, the velocity seen by the Fabry-Pérot interferometer is the projection of the ions velocity upon the line of sight. Therefore, the Doppler shift that has to be taken into account in the model corresponds to the projection of the velocity vector upon the line of sight. Thus:

$$v_{projected} = \sqrt{v_{axial}^2(\alpha,R) + v_{radial}^2(\alpha,R)} \cdot \cos(\theta-\alpha) \tag{8}$$

Then,

$$\delta\nu_D = \frac{v_{projected}}{\lambda_0} \tag{9}$$

At this stage, the three quantities needed to solve Eq.1 are either known or estimated. Note that a constant is fixed in order to simulate the presence of low velocity ions. However, in order to obtain the complete interference pattern, it is necessary to take into account the Fabry-Pérot interferometer Apparatus function whose FWHM depends on the spectral resolution of the setup. It has been experimentally measured at 3 GHz. Therefore, the computed signal is the convolution of the interference pattern and an Airy function *A* (which is the shape of the Apparatus function of a Fabry-Pérot interferometer):

$$I(\nu) = \left( \sum_z \sum_r \frac{n(z,r)}{\Delta\nu_D} e^{-\ln(2)\cdot\left(\frac{\nu-\delta\nu_D}{\Delta\nu_D}\right)^2} \right) \otimes \mathrm{A}(\nu) \tag{10}$$

The ion velocity evolves continuously as ions move away from the thruster exit and/or the channel axis. Therefore, each point of an interference pattern can be seen as the contribution of a $Xe^+$ ions velocity group or could be if we could get rid of the Apparatus function and if the $Xe^+$ ions spectral line at 541.9 nm was a Dirac function. However, providing that the $Xe^+$ ion velocity groups are limited enough in space on the projected velocity map, the top of the second peak should still corresponds to the velocity group whose density is the greatest, which can be located thanks to the Abel transform of the thruster picture. This assumption can be proved to be false if the $Xe^+$ ions density and/or the projected velocity displays a small gradient in the direction of the line of sight. The density gradient can be measured through the Abel transform of the thruster picture, but

the velocity gradient is what we seek to measure. Moreover, even if the velocity map contains limited velocity groups in space (i.e. an important gradient), the projection of this map along the line of sight could still lead to extensive projected velocity groups, without us being able to predict it.

Thus, a velocity profile can only be extrapolated from interference patterns measurements by making the assumption that the above conditions are met. As can be seen in Fig.6, the gradient of the measured velocity profiles would be strong enough to prove our assumption to be true, but the velocity profile is relevant only if the assumption is proven first. However, since the density and velocity maps vary with the thruster parameters, there is no way to do that.

**D. Check of the validity of velocity profiles**

The two dimensional model is able to produce a theoretical two dimensional velocity map from a velocity modulus profile in the axial direction (which is what our measured profiles are supposed to be). Then, the corresponding interference patterns can be calculated depending on the position of the line of sight. Even though the plasma plume is modeled as an expanding jet, it is expected that it is still a good approximation of the plasma behavior. The expanding jet divergence has not been determined arbitrarily though. Hybrid simulations showed that such a divergence was typically equal to 30°, which is confirmed by the Abel transforms of our pictures taken by CCD camera.

The measured velocity profiles have been entered in the model to calculate the corresponding velocity map (and interference patterns) in order to check if the calculated and measured interference patterns would match. As can be seen in Fig.5, the agreement between experiments and theory is quite good, providing that the line of sight does not intercept the interior of the channel (because the model only computes the plasma plume behavior outside the thruster). This would not be sufficient if the top of the calculated interference patterns did not correspond to the velocity group whose density is the greatestt, but the distance between this velocity group and the one corresponding to the top of the peak is less than 2 mm (in the axial direction) in the worst cases. Note that the relative spatial resolution has also been experimentally measured to be better than 2 mm.

It is also interesting to know that each interference pattern contains information about the whole ion velocity distribution in space through its shape, whatever the position of the line of sight is. Indeed, the locations of the different velocity groups are lost when the signal collected by the Fabry-Pérot interferometer is integrated along the line of sight, but the shape of the interference patterns still contain information about the velocity groups contained in the line of sight. Therefore, even though the location of a single velocity group is recovered thanks to CCD imaging, the other groups allow to validate experimental velocity profiles.

In other words, an experimental profile is validated if for every point in the profile, every computed interference patterns match the experimental ones.

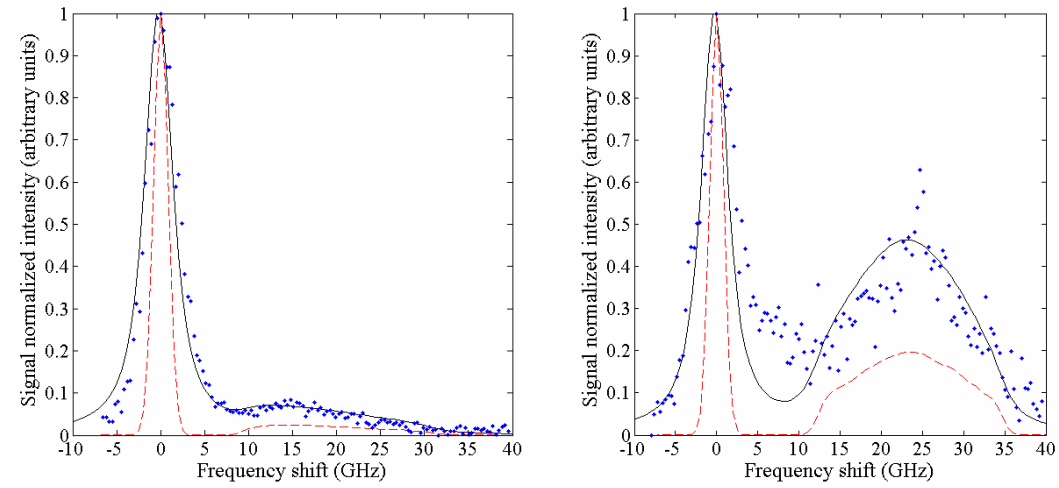


**Figure 5. Calculated interference patterns convoluted (full lines) and not convoluted (dashed lines) with the Apparatus function compared to experimental measurements (points). Left curves: line of sight position = 2 mm. Right curves: line of sight position = 20 mm. Thruster parameters: $U_d$ = 550 V, and $\Phi_a$ = 8.6 mg.s$^{-1}$.**

### E. Summary of the technique

The FP interferometry technique discussed in this paper is not about extracting directly a velocity profile from interference patterns measurements. On the contrary, it is sought to determine this velocity profile thanks to a numerical simulation so that the computed interference patterns match the measured ones. Each point from the velocity profile corresponds to a different interference pattern measured for different locations of the line of sight.

Each interference pattern provides a direct measurement of the Doppler shift which in turn leads to an estimation of the $Xe^+$ ion velocity. Since the signal measured by Fabry-Pérot interferometry is integrated in space, it is not possible to tell the location of these ions from the interference patterns alone. However, each measured velocity is linked to a location of the line of sight which is known because of the travel stage.

Then, by using a two dimensional density map (i.e. the Abel transfom of a thruster picture taken by a CCD camera), it is possible to determine the locations of the highest density points corresponding to each line of sight. It is then assumed that these are also the locations of the ions corresponding to the measured velocities. Therefore, one obtains a velocity profile (see Fig.6).

Finally, this velocity profile is used by the two dimensional model to simulate the shape of the interference patterns corresponding to each experimental location of the line of sight. The velocity profile is validated if every simulated interference patterns match the measured ones.

Note that it is not known during the measurements what is the location of the velocity group that corresponds to the top of the second peak. It is even likely that for a given location of the line of sight, the location of the $Xe^+$ ion group corresponding to the top of the second peak changes with the thruster parameters.

## IV. Results interpretation

As already mentioned, the first result of these measurements is that there are ions with low velocity in the plasma plume. They may be created by charge exchange between fast $Xe^+$ ions and slow Xe atoms (see Eq.11). However, the location of these ions is still unknown, but their velocity can be estimated at less than 1 $km.s^{-1}$. Indeed, as can be seen in Fig.5, the first peak of the experimental interference pattern is slightly shifted from the first peak of the calculated one. Yet, the velocity of these slow ions has been fixed to 0 in the model. The difference between the two patterns means there is a contribution from a group of ions whose velocity leads to a weak Doppler shift (<1 GHz), hence the previous estimation. Note that in the simulations, the quantity of low velocity ions is fixed so that the computed interference patterns match the experimental ones.

$$Xe^+_{fast} + Xe_{slow} = Xe^+_{slow} + Xe_{fast} \tag{11}$$

The velocity error bars in Fig.6 are standard deviation resulting from series of measurement, whereas the distance error bars represent the gap between the location of the highest density point and the location of the velocity group corresponding to the top of the second peak. Of course, the distance error bars can be estimated only thanks to the two dimensional model. However, the distance error bars are of the same order of magnitude

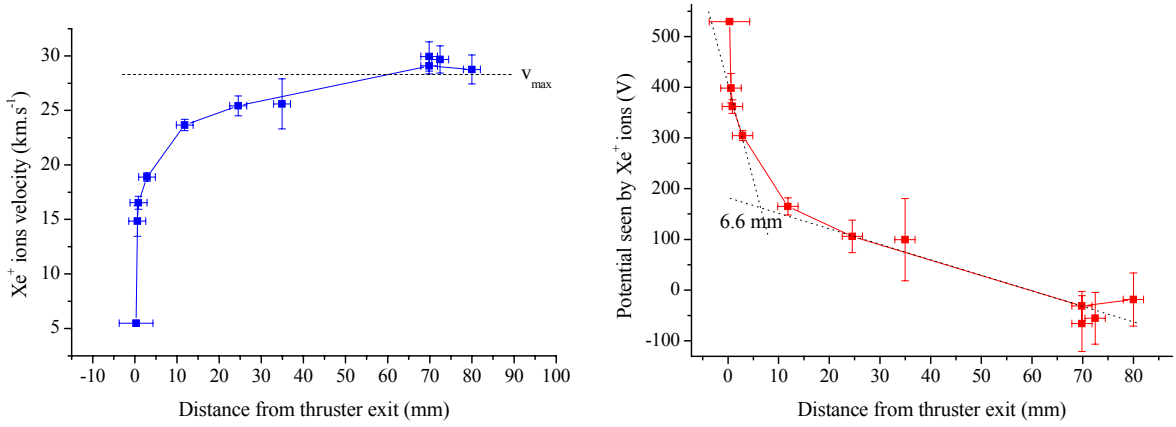


**Figure 6. To the left: $Xe^+$ ion velocity profile (the dashed line represents the maximum velocity that can be reached by the ions). To the right: accelerating potential seen by the $Xe^+$ ions. Thruster parameters for both curves: $U_d$ = 550 V, and $\Phi_a$ = 8.6 $mg.s^{-1}$.**

than the experimental resolution. Note that the profile point at 0 mm displays a more important error bar because it is difficult to determine whether this point is really located at the thruster exit or inside the thruster channel.

The potential seen by $Xe^+$ ions is calculated from the velocity profile by making the assumption that there is no energy transfer through collisions (see Eq.12).

$$U_{acc} = U_d - \frac{1}{2 \cdot e} \cdot m_{Xe} \cdot v^2 \tag{12}$$

As can be seen in Fig.6, the ion velocity profile displays two regimes which translate into linear regimes for the accelerating potential. The discontinuity between these two regimes occurs at ~ 6.6 mm. This behavior is coherent with previous Fabry-Pérot and LIF measurements carried out on a SPT-100 HET two years ago [4], as can be seen in Fig.7.[6] Note that the Fabry-Pérot diagnostic tool used at that time was not as evolved as the one described in this paper, but still allowed a good agreement between LIF and Fabry-Pérot data.

Until now, the hybrid model developed at CPAT relied on the assumption that inside the thruster channel, the "anomalous" electron mobility was proportional to $1/B^2$ ($B$ being the magnetic field) due to secondary electrons produced by interactions between electrons and the $BNSiO_2$ walls. Outside the thruster channel, turbulent electric field is assumed to cause the "anomalous" electron mobility (which is then proportional to $1/B$) since wall collisions cannot be expected to be of importance beyond the channel exhaust[7]. The frontier between these two regimes was supposed to be located at the thruster exhaust. Figure 4 shows that a discontinuity between two regimes indeed exists, but that it is located outside the thruster channel. Thus, it is possible that electron-wall interactions do not cause the anomalous electron mobility inside the channel because the corresponding regime occurs inside and outside the channel (the LIF data shown in Fig.7 confirm there is no discontinuity caused by the $BNSiO_2$ channel), even though this possibility cannot be dismissed. However, turbulent electric field alone could also explain the "anomalous" electron conductivity outside the channel as well as inside. More works is needed to understand the "anomalous" mechanisms of cross-field electron transport.

Furthermore, it has been possible to show that the potential drop seen by the $Xe^+$ ions occurs mainly outside the thruster. To this end, the PPS X000-ML HET has been operated over a various set of parameters: from 200 V to 1000 V applied voltage, which correspond to power varying from 2 kW to 6 kW; and from 5 mg/s to 15 mg/s Xe mass flow rate, with different magnetic configurations (in each case the magnetic configuration has been optimized to minimize $I_d$). For each set of parameters, two interference patterns have been measured; the first one corresponding to a line of sight intercepting the inside of the thruster channel, whereas the second interference pattern corresponds to a line of sight intercepting the plasma plume only. As can be seen in Fig.8, the potential drop typically occurs at ~ 70% outside the thruster channel (complete velocity profiles would be needed to reduce the error bars), even though it has not been possible to highlight tendencies in the evolution of this percentage with the thruster parameters.

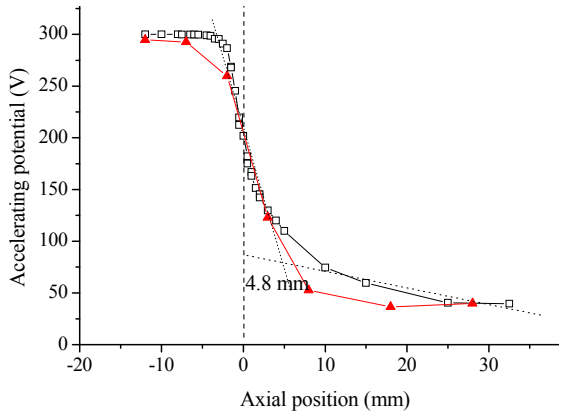


**Figure 7. Development of the accelerating potential along the channel axis of a SPT-100 HET: Fabry-Pérot measurements (triangle) and LIF data (square). Thruster parameters: $U_d$ = 300 V, $\Phi_a$ = 5.42 mg.s$^{-1}$.**

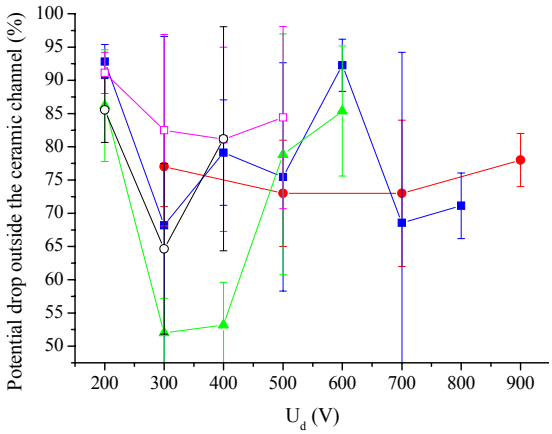


**Figure 8. Potential drop outside the thruster channel as a function of $U_d$ for different mass flow rates: $\Phi_a$ = 5 mg.s$^{-1}$ (full circle), $\Phi_a$ = 6 mg.s$^{-1}$ (full square), $\Phi_a$ = 8 mg.s$^{-1}$ (full triangle), $\Phi_a$ = 11 mg.s$^{-1}$ (hollow square) and $\Phi_a$ = 15 mg.s$^{-1}$ (hollow circle).**

## V. Conclusion

We now have the use of a non intrusive and an easy to implement diagnostic tool made of a Fabry-Pérot interferometer a CCD camera and a two dimensional numerical model. Numerous data can be retrieved even though data treatment proves to be quite complex. Measuring several interference patterns near the thruster exit is compulsory though, since the location of the frontier between the two conductivity regimes, which is an important issue to eventually modeling HET behavior, varies with thruster parameters or magnetic configuration.

This technique allowed to demonstrate the presence of low velocity ions in the plasma plume of a HET and to localize the frontier between two conductivity regimes outside the thruster.


## Aknowledgment

This work is carried out in the frame of the research group CNRS/CNES/SNECMA/Universities 2759 "Propulsion Spatiale à Plasma".


## References


[1] R.F.G. Meulenbroeks, P.A.A. van der Heijden, M.C.M. van de Sanden, D.C. Schram, "*Fabry-Pérot line shape analysis on an expanding cascaded arc plasma in argon*", J. Appl. Phys. **75**, 2775, 1994.

[2] C.J. Timmermans, A. Lunk, D.C. Schram, "*The rotation of ions and neutrals in a cylindrical magnetized hollow cathode argon arc*", Contr. Plasma Physics 21, **117**, 1981.

[3] S. Mazouffre, D. Pagnon, P. Lasgorceix, M. Touzeau, "*Temperature of xenon atoms in a stationary plasma thruste*r", Proceedings of the 28th International Electric Propulsion Conference, Toulouse, France, paper **283**, 2003.

[4] S. Mazouffre, D. Pagnon and J. Bonnet, "*Two ways to evaluate the Xe+ ion flow velocity in a Hall effect thruster – LIF spectroscopy and Fabry-Pérot interferometry*", AIAA paper **04-3949** (2004).

[5] S.N. Askhabov, M.PM Burgasov, A.N. Veselovzorov et al. "*Issledovanie strui stacionarnogo plasmennogo uskoritelya s zamknutym dreifom electronov (UZDP)*" Physika Plasmy **7**(1), 225 (1981) ["*Study of the plume of a stationary plasma accelerator with closed electron drift (UZDP)*", Fizika Plasmy ]

[6] N. Dorval, J. Bonnet, J. P. Marque, E. Rosencher, S. Chable, F. Rogier, P. Lasgorceix, "*Determination of the ionization and acceleration zones in a stationary plasma thruster by optical spectroscopy study: Experiments and model*", J. Appl. Phys. Vol. **91**, No. 8 , pp 4811 – 4817 (2002)

[7] G. J. M. Hagelaar, J. Bareilles, L. Garrigues, and J.-P. Bœuf, "*Role of anomalous electron transport in a stationary plasma thruster simulation*", J. Appl. Phys., Vol. **93**, No. 1, pp 67 – 75 (2003)